

# In-hand manipulation of a circular dynamic object by soft fingertips without angle measurement

R. GARCIA-RODRIGUEZ<sup>1\*</sup> & V. PARRA-VEGA<sup>2</sup>

<sup>1</sup>*Aeronautical Engineering Program and Postgraduate Program in Aerospace Engineering,  
Universidad Politécnica Metropolitana de Hidalgo, Hidalgo 43860, Mexico;*

<sup>2</sup>*Robotics and Advanced Manufacturing Department, Research Center for Advanced Studies (CINVESTAV),  
Unidad Saltillo 25900, Mexico*

Received 12 May 2020/Revised 6 July 2020/Accepted 1 September 2020/Published online 8 April 2021

**Abstract** A multi-fingered robotic hand with curved fingertips enables contact re-positioning without reattaching at the expense of fingertip rolling. This rolling stands for a characteristic that facilitates dexterous manipulation but results in an algebraically complex dynamic model subject to such constraints. The hemispherical shape of fingertips allows a dexterous manipulation when controlling the tangential forces, which are essential to rotate object. However, the measurement of the object angle in practice requires tactile-optical sensing. In this paper, considering robotic fingers with curved soft tips, we propose a feedback control that ensures optimal dynamical grasping of a circular rigid object. It is shown that the collaboration of the contact forces, to get a minimum pose of internal forces, and the tangential forces, to induce the conditions for assuring the grasp closure, is necessary to get a skillful manipulation. In this case, the orientation control of a circular object to the desired angle while avoiding direct measurement of the object angle is presented. Stability conditions of the system are presented in the sense of stability-in-the-manifold. Finally, representative simulations are shown and discussed.

**Keywords** optimal grasping, manipulation, soft-fingertips, circular object, stability-in-the-manifold

**Citation** Garcia-Rodriguez R, Parra-Vega V. In-hand manipulation of a circular dynamic object by soft fingertips without angle measurement. *Sci China Inf Sci*, 2021, 64(5): 152209, <https://doi.org/10.1007/s11432-020-3059-9>

## 1 Introduction

Some human manipulation tasks, such as squeezing a small ball, screwing, rolling an object, or re-positioning a pen in hand, are characterized by fingertip pinching rather than through hand movement [1, 2]. This ability, to hold and move an object using the fingers, can be explained by the synergistic work of two fundamental forces applied onto the object at the fingertip location: contact forces and tangential forces. Controlling these forces precisely is very difficult, which may be one reason why robotic hands present a limited ability and low performance when considering the frictionless rigid contact point (CP) approaches [3, 4]. The manipulation tasks based on point contact establish an infinitesimally small point (as if touching with needles), neglecting the dynamical contribution of the tangential forces, appearing alone when the friction cone is artificially considered [5, 6]. In this way, a vast amount of studies have explored the ability of robotic hands subject to traditional assumptions such as hard fingertips and CP under non-rolling and non-sliding contacts [7, 8]. In practice, the CP approach is typically violated, introducing contact pads to increase the contact area (CA) and the static coefficients, so this practice lacks any theoretical support. At this point, it is reasonable to ask: why are CP-based manipulations the most popular approach to synthesize them? There may be many reasons, but we conjecture that from a theoretical perspective, it is less challenging to implement than CA-based robotic hands.

A more realistic design, to reproduce some human manipulation tasks, is to consider a robotic finger with a tip of rigid hemispherical shape (let us call it S-finger). In this way, a rigid rolling motion is induced, removing the limitation of fingertip re-positioning. Robotic hands with S-fingers have been

\* Corresponding author (email: [rogarcia@upmh.edu.mx](mailto:rogarcia@upmh.edu.mx))

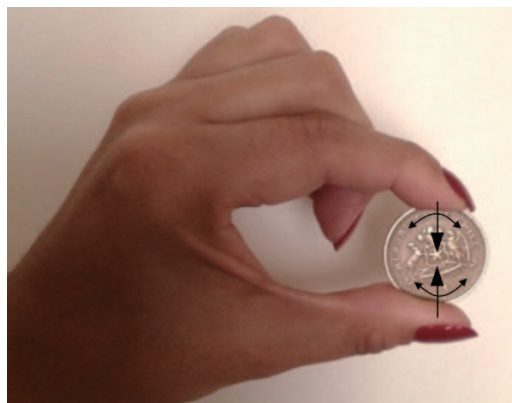


**Figure 1** (Color online) Grasp and orientation of a circular object by pads of the thumb and index fingers.

used to deal with rigid uncertain environments [9] and compliant (deformable) environments [10], while in [11], experiments for a simple 2-finger hand with 1 degree of freedom (DoF) for each finger are presented. Additionally, some control schemes based on S-fingers have proved useful for the manipulation of planar objects [12–16]. Hence, S-fingers can be considered as elements to increase the skill of robotic hands where the rolling and the CP<sup>1)</sup> are involved [17].

Dexterous manipulation in humans (i.e., hand manipulation) results from fingers with a hemispherical shape and soft tip. The seminal paper [18] introduces the CA approach by soft fingertips deforming at contact while performing rolling motion as S-fingers. Let us call them SD-fingers. The design of soft fingertip and hemispherical shape allows understanding and exploiting more intuitively the joint work between the rolling motion and the fingertip's deformation through tangential forces and contact forces, respectively [19]. Despite the apparent dynamic model complexity, the instrumental approach suggests that redundant robotic fingers are necessary to guarantee a large enough manifold to satisfy the control objectives. This formulation allows a new kind of dexterous manipulation where independent controls for contact and tangential forces [20,21] are proposed. Complementary to this, the superposition principle [22,23] can be used to design a control structure based on the sum of synergies. A complete contact model to grasp and manipulate a planar object was presented in [24]. Recently, it has been pointed out that visual manipulation using SD-fingers can be guaranteed; that is, the delay in the visual loop can be compensated, if fast sensory feedback is provided [25]. Using the virtual object concept [8], in [26] the manipulation of an arbitrary shape object was shown. However, the contribution of tangential forces is not taken into account owing to the assumption of rigid point contact with the classical DAE-2 formulation [18], given that it still depends on the friction cone. In [27–31], the manipulation of a circular object using redundant SD-fingers is showed. In [32], grasping and manipulation using redundant SD-fingers considering the gravity effect was presented. Exploiting the rolling motion via SD-fingers was used in [16], where the force control angle optimization for grasping is shown, assuming that the gravity force is zero. Although grasp quality has been extensively studied for rigid contact [33–36], it has been vastly ignored for soft or deformable contact despite successful testing [37,38]. The advantages of SD-fingers seem not eloquent enough to attract attention, not only for manipulation but also for hand-manipulation. This is mainly because model complexity looks too challenging to deal with in practice and due to a lack of formal stability analysis and physical measurements, which require experimental tactile-optical sensing [39] or massive tactile sensor data [40,41]. As a result, few studies have focused on the in-hand manipulation via SD-fingers.

**Contribution.** For the in-hand manipulation, such as turning a circular object, the opposition between thumb and index finger is crucial. The rolling motion is used to rotate the object while the oppositional forces compensate for the external forces and torque [42]; see Figure 1. Additionally, we can notice that in the precision grip of a circular object, using the thumb and index fingers, the active touch information plays a more critical role over visual sensor information. Contrary to traditional approaches where the object angle is measured through sensors or by using state estimators and considering the natural finger movement, an optimal dynamical grasping and orientation control mechanism using SD-fingers, avoiding the measurement of the angle, is proposed. The optical grasping condition is achieved

1) CP explicitly assumes that contact occurs at an infinitesimally small static contact point.

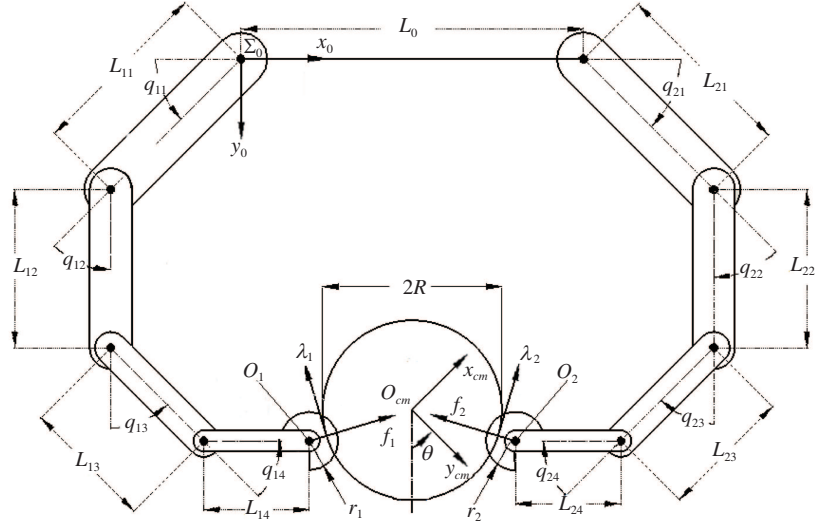


**Figure 2** Kinematics of hemispherical soft-fingertip hand grasping a circular object.

when the contact forces, through the tangential forces, are aligned dynamically to reach the restraint conditions. Simultaneously, the orientation of a circular object is achieved using a potential-shaping control mechanism where the object orientation is approximated by a kinematic relationship between the fingertips. Thus, the tangential forces play a fundamental, through the rolling, to get a dexterous manipulation. For the best of our knowledge, it is the first time this result has been reported. Finally, the effect of synergies for pose regulation of a circular object can be seen in [43, 44].

**Organization.** This paper is organized as follows. Dynamical equations of the constrained robotic system and restraint conditions are presented in Section 2. In Section 3, the optimal grasping and orientation controller for manipulating a circular object is presented. Simulation results show the viability of our approach under various conditions in Section 4. Finally, in Section 5 the conclusion is addressed.

## 2 Constrained dynamical model

Consider a robotic hand of two planar fingers with four DoFs for each finger, whose end-effectors are equipped with a hemispherical lossless deformable homogeneous material, operating in the elastic regime. It is assumed that robotic fingers are holding firmly a rigid circular object; see Figure 2, where  $\Sigma_0$  stands for the fixed/inertial coordinate frame,  $O_{cm} = [x, y]^T$  is the center mass of the object, while  $O_1 = [x_1, y_1]^T$  and  $O_2 = [x_2, y_2]^T$  are the center of fingertips, respectively. In addition, the generalized positions of the robotic fingers and the rigid object are defined as  $\mathbf{q}_i = [q_{i1}, q_{i2}, q_{i3}, q_{i4}]^T \in \mathbb{R}^4$  and  $[\bar{\mathbf{p}}^T, \theta]^T \in \mathbb{R}^3$ , respectively.

### 2.1 Contact force and rolling motion

The maximum radial deformation of the  $i$ -th fingertip,  $\delta_i \in \mathbb{R}$ , can be obtained by measurable data as

$$\delta_i = \delta_i(\mathbf{q}_i, \bar{\mathbf{p}}) = \bar{R} + (-1)^i (C_{x_i} - C_{y_i}), \quad (1)$$

where  $\bar{R} = r_i + R \in \mathbb{R}$ ,  $C_{x_i} = (x - x_i)c_i$ ,  $C_{y_i} = (y - y_i)s_i$  with  $s_i = \sin(\alpha_i) \in \mathbb{R}$ ,  $c_i = \cos(\alpha_i) \in \mathbb{R}$ , and  $\alpha_i \doteq \alpha_i(\mathbf{q}_i, \bar{\mathbf{p}}) = \tan^{-1}(X_i(\mathbf{q}_i, \bar{\mathbf{p}})) \in \mathbb{R}$  represents the angle between the  $i$ -th normal force vector and the horizontal for  $X_i(\mathbf{q}_i, \bar{\mathbf{p}}) = -(\frac{y-y_i}{x-x_i}) \in \mathbb{R}$ ; see Figure 3. As is pointed in [21], the  $i$ -th normal force  $f_i \in \mathbb{R}$  can be defined as a function of the deformation at the fingertip, that is,

$$f_i = f_i(\delta_i, \bar{\mathbf{p}}) = k\delta_i^2, \quad (2)$$

where  $k = 2\pi E \in \mathbb{R}$  is the fingertip stiffness with  $E \in \mathbb{R}$  representing the Young modulus of the soft material. For circular objects, the maximum normal force applied to the object occurs at the contact point  $P_c$  located along the line connecting the center of the fingertip base with the center of mass of the object,  $\text{CoM}_o$ ; see Figure 3.

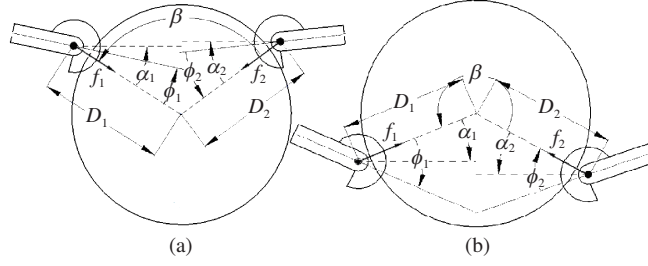


**Figure 3** Kinematic relationships at contact, where the normal force relative angle  $\beta(\bar{\nu}) = \alpha_1 - \alpha_2 + \pi \in \mathbb{R}$  is depicted. All angles are measured according to the right-hand rule and being consistent with the inertial frame, i.e., in (a)  $\alpha_1 < 0$ ,  $\alpha_2 > 0$ ,  $\phi_1 < 0$ ,  $\phi_2 < 0$ , and for (b)  $\alpha_1 > 0$ ,  $\alpha_2 < 0$ ,  $\phi_1 > 0$ ,  $\phi_2 > 0$ .

On one hand, notice that when the fingertip is in contact with the object it is subject to a kinematic constraint [17],  $\phi_i = \phi_i(\mathbf{q}_i, \bar{\mathbf{p}}) = \pi - (-1)^i \alpha_i - \mathbf{q}_i^T \mathbf{e}_i \in \mathbb{R}$ ,  $\mathbf{e}_i = [1, 1, 1, 1]^T \in \mathbb{R}^4$ ,  $i = 1, 2$ , and then its hemispherical shape induces a rolling velocity constraint given by  $(-1)^i R \dot{\theta} = -r_i \dot{\phi}_i$  with respect to the inertial frame. Thus, the (differentiable) velocity constraint owing to hemispherical  $i$ -th finger at contact can be expressed as follows [4]:

$$\dot{\varphi}_{r_i} = (-1)^i R \frac{d}{dt} \theta + r_i \frac{d}{dt} \phi_i = 0, \quad (3)$$

where  $\dot{\varphi}_{r_i} = \dot{\varphi}_{r_i}(\mathbf{q}_i, \bar{\mathbf{p}})$ . Considering that Eq. (3) is integrable, the vector-valued solution  $\varphi_{r_i} \in \mathbb{R}$  is given as

$$\varphi_{r_i} = (-1)^i R \theta + r_i \phi_i + C_{\varphi_{r_i}} = 0, \quad (4)$$

where  $\varphi_{r_i} = \varphi_{r_i}(\mathbf{q}_i, \bar{\mathbf{p}})$ , and  $C_{\varphi_{r_i}} = C_{\varphi_{r_i}}(R, r_i, \theta(t_0), \phi_i(t_0)) \in \mathbb{R}$  stands for an integration constant at the initial condition. Notice that  $\phi_1(\mathbf{q}_1, \bar{\mathbf{p}})$  is measured from the first normal force vector to the collinear vector to the last link, and  $\phi_2(\mathbf{q}_2, \bar{\mathbf{p}})$  is measured from the collinear vector to the last link to the second normal force vector.

## 2.2 Dynamic model

Let  $K = K(\mathbf{q}, \dot{\nu}) \in \mathbb{R}$  be the kinetic energy of the system that in fact becomes  $K = \sum_{i=1}^2 K_i + K_0$ , where  $\mathbf{q} = [\mathbf{q}_1^T, \mathbf{q}_2^T]^T \in \mathbb{R}^8$ ,  $\dot{\mathbf{q}} = [\dot{\mathbf{q}}_1^T, \dot{\mathbf{q}}_2^T]^T \in \mathbb{R}^8$ ,  $\nu = [\mathbf{q}^T, \mathbf{p}^T]^T \in \mathbb{R}^{11}$ , and  $\dot{\nu} = [\dot{\mathbf{q}}^T, \dot{\mathbf{p}}^T]^T \in \mathbb{R}^{11}$  are the generalized coordinates of positions and velocities of the system, respectively;  $K_i = \frac{1}{2} \dot{\mathbf{q}}_i^T H_i(\mathbf{q}_i) \dot{\mathbf{q}}_i \in \mathbb{R}$  stands for the kinetic energy of the rigid  $i$ -th robot manipulator,  $H_i(\mathbf{q}_i) \in \mathbb{R}^{4 \times 4}$  is the inertial positive definite matrix,  $K_0 = \frac{1}{2} \dot{\mathbf{p}}^T H_0 \dot{\mathbf{p}} \in \mathbb{R}$  represents the kinetic energy of the circular object, with  $H_0 = \text{diag}(m, m, I) \in \mathbb{R}^{3 \times 3}$  being the constant object inertial matrix. Parameters  $m \in \mathbb{R}$ , and  $I = I_{zz} \in \mathbb{R}$  represent the mass, and the mass moment of inertia of the object, respectively. Considering that the system is under the gravity effect, the potential energy of the system  $P \in \mathbb{R}$  is defined as

$$P(\nu) = \sum_{i=1}^2 P_{G_i}(q) + P_{G_o}(y) + \sum_{i=1}^2 P_{E_i}(\delta_i), \quad (5)$$

where  $P_{G_i}(q) \in \mathbb{R}$  and  $P_{G_o}(y) \in \mathbb{R}$  are the generalized potential energies induced by the Earth's gravitational field onto the  $i$ -th finger and onto the object, respectively, while  $P_{E_i}(\delta_i) = \frac{1}{3} \pi k \delta_i^3 \in \mathbb{R}$  stands for the elastic potential energy at contact of the  $i$ -th fingertip. Integrating  $P_{E_i}(\delta_i)$  from the  $i$ -th normal force  $f_i(\delta_i)$  yields  $P_{E_i}(0) = \frac{1}{3} k \delta_i^3(0)$  which represents the initial elastic potential energy at contact. Applying the variational principle to the constrained Lagrangian,  $L_r(\nu, \dot{\nu}) = L + S_t$ , we have that

$$\int_{t_1}^{t_2} [\delta L + \varphi_r^T \lambda + \mathbf{u}^T \delta \nu] dt = 0, \quad (6)$$

where  $L = K(\mathbf{q}, \dot{\nu}) - P(\nu)$  represents the Lagrangian,  $S_t = \sum_{i=1}^2 \varphi_{r_i} \lambda_i$  is the rolling constraint of the system with  $\lambda_i \in \mathbb{R}$  being the magnitude of the tangential force at the contact point of the  $i$ -th fingertip, and  $\mathbf{u}$  is the input vector for torque control. The solution of (6), according to the Euler-Lagrange modeling formalism becomes

$$\frac{d}{dt} \left[ \frac{\partial}{\partial \dot{\nu}} L \right] - \frac{\partial}{\partial \nu} L - \frac{\partial}{\partial \nu} (\varphi_r^T \lambda) = \mathbf{u}, \quad (7)$$

where  $\varphi_r = [\varphi_{r_1}, \varphi_{r_2}]^T \in \mathbb{R}^2$  and  $\lambda = [\lambda_1, \lambda_2]^T \in \mathbb{R}^2$  are the vectors of rolling constraints, and Lagrangian multipliers, respectively; while  $\mathbf{u} = [\boldsymbol{\tau}_1^T, \boldsymbol{\tau}_2^T, \boldsymbol{\tau}_o^T]^T = [\boldsymbol{\tau}_1^T, \boldsymbol{\tau}_2^T, \mathbf{0}^T]^T \in \mathbb{R}^{11}$ . Solving (7), the dynamic equations of the robotic fingers and the object are defined as

(Dynamics of the  $i$ -th finger)

$$\mathbf{H}_i(\mathbf{q}_i)\ddot{\mathbf{q}}_i + \mathbf{C}_i(\mathbf{q}_i, \dot{\mathbf{q}}_i)\dot{\mathbf{q}}_i + g_i(\mathbf{q}_i) = \boldsymbol{\tau}_i + (-1)^i f_i \mathbf{J}_i^T(\mathbf{q}_i) \begin{bmatrix} c_i \\ -s_i \end{bmatrix} + r_i \left( \mathbf{J}_i^T(\mathbf{q}_i) D_i^{-1} \begin{bmatrix} s_i \\ c_i \end{bmatrix} - \mathbf{e}_i \right) \lambda_i, \quad (8)$$

(Under-actuated object dynamics)

$$\mathbf{H}_0 \ddot{\mathbf{p}} + g_0(\mathbf{p}) = \boldsymbol{\tau}_o + \sum_{i=1}^2 \left( (-1)^i f_i \begin{bmatrix} -c_i \\ s_i \\ 0 \end{bmatrix} \right) + \sum_{i=1}^2 \left( (-1)^i R \begin{bmatrix} 0 \\ 0 \\ 1 \end{bmatrix} - r_i D_i^{-1} \begin{bmatrix} s_i \\ c_i \\ 0 \end{bmatrix} \right) \lambda_i, \quad (9)$$

where  $\mathbf{C}_i(\mathbf{q}_i, \dot{\mathbf{q}}_i)$  stands for the Coriolis matrix,  $g_i(\mathbf{q}_i)$  and  $g_0(\mathbf{p}) = [0, -Mg, 0]^T$  are the gravitational torque vectors for the  $i$ -th finger and the object, respectively,  $\mathbf{J}_i^T(\mathbf{q}_i)$  is the Jacobian matrix, and  $D_i = D_i(\mathbf{q}_i, \bar{\mathbf{p}}) = \|\bar{\mathbf{x}}_i(\mathbf{q}_i) - \bar{\mathbf{p}}\|_2 > 0$  is the distance from CoM<sub>o</sub> to the base center position of the  $i$ -th deformable fingertip with  $\bar{\mathbf{x}}_i = [x_i, y_i]^T \in \mathbb{R}^2$ .

**Remark 1.** The fact that  $\boldsymbol{\tau}_o = [0, 0, 0]^T \in \mathbb{R}^3$  in (9) means that the object motion is under-actuated. That is, the object position  $\mathbf{p}$  can be modified only indirectly, through controlling the external forces applied to the object, given by  $f_i(\delta_i) \in \mathbb{R}^2$  and  $\lambda_i \in \mathbb{R}^2$ . Thus, the control of  $(f_i(\delta_i), \lambda_i)$  is fundamental to guarantee object manipulation.

**Remark 2.** Force terms  $f_i(\delta_i)$  and  $\lambda_i$  are complementary, belonging to orthogonal complements, while

$$c_i = \cos(\alpha_i) = \frac{1}{\sqrt{X_i^2(\mathbf{q}_i, \bar{\mathbf{p}}) + 1}} = -(-1)^i \left( \frac{x - x_i}{D_i} \right)$$

and

$$s_i = \sin(\alpha_i) = \frac{X_i}{\sqrt{X_i^2(\mathbf{q}_i, \bar{\mathbf{p}}) + 1}} = -(-1)^i \left( \frac{y_i - y}{D_i} \right)$$

are used to obtain the object angle, avoiding the direct object angle measurement  $\theta$  as is reported frequently in the literature. Thus, the control orientation of a circular object can be carried out without any sensor.

**Remark 3.** In virtue of  $r < R$ , it is reasonable to assume that  $-\frac{\pi}{2} \leq \alpha_i(\mathbf{q}_i, \bar{\mathbf{p}}) \leq \frac{\pi}{2}$ ; see Figure 3.

To elucidate an optimal manipulation by the robotic fingers with soft fingertips, some structure properties of the model are now analyzed.

### 2.3 Structure properties

#### 2.3.1 Primary manifold

The state-space is constrained by the rolling constraint (4), which gives rise to the so-called primary constrained manifold  $\mathcal{M}_{\varphi_r}$ , defined by

$$\mathcal{M}_{\varphi_r} = \{(\boldsymbol{\nu}, \dot{\boldsymbol{\nu}}) \in \mathbb{R}^{22} : \varphi_{r_i} = 0, \dot{\varphi}_{r_i} = 0\}, \quad i = 1, 2, \quad (10)$$

where  $\dot{\boldsymbol{\nu}} = [\dot{\mathbf{q}}^T, \dot{\mathbf{p}}^T]^T \in \mathbb{R}^{11}$  with  $\dim(\mathcal{M}_{\varphi_r}) = 18$ . Despite the fact that the state space vector is of dimension 22,  $\dim(\mathcal{M}_{\varphi_r})$  is reduced because there exists two constraints on position and two on level velocity [18]. Thus, initial conditions and desired trajectories must comply to such constraints, for consistency of the DAE-2 [45].

#### 2.3.2 Passivity

Assume the input-output pair  $\langle u, y \rangle$ , with  $u = (\tau_i, \tau_o) \in \mathbb{R}^{11}$  as input torque and  $y = (\dot{q}, \dot{p}) \in \mathbb{R}^{11}$  as the velocity output. Then, Ref. [27] shows that the energy balance  $\langle u, y \rangle = \frac{d}{dt} \mathcal{H} = 0$  in virtue of (4), where  $\mathcal{H}(\boldsymbol{\nu}, \dot{\boldsymbol{\nu}}) = K(\boldsymbol{\nu}, \dot{\boldsymbol{\nu}}) + P(\boldsymbol{\nu}) \in \mathbb{R}$ . That is, in the open loop the constraint forces along the variational of the constraints vanish; for a storage function  $\mathcal{H}(\boldsymbol{\nu}, \dot{\boldsymbol{\nu}})$ , consequently the integral of  $\mathcal{H} = 0$  yields  $\mathcal{H}(t_f) = \mathcal{H}(t_0)$ , showing a passive lossless system.

### 2.3.3 Joint friction endows dissipativity

The analysis above yields  $\langle u, y \rangle = \dot{\mathcal{H}} = -\xi$ , for  $\xi = \dot{\nu}B\dot{\nu} > 0$  when the robotic finger has viscous friction  $B\dot{\nu}$  at each joint, for  $B > 0$ . Then, its integral yields  $\mathcal{H}(t_f) = \mathcal{H}(t_0) - \bar{\xi} < \mathcal{H}(t_0)$ , for  $\bar{\xi} = \int_{t_0}^{t_f} \xi > 0$ , showing that the system is a dissipative system, with dissipation energy rate of  $\xi$ .

## 2.4 Constraint conditions on the grasped object

To guarantee that the circular object is grasped securely over the task [42, 46], a firm grip is required and thus contact constraint forces are not arbitrarily set. The object's dynamics (9) becomes, under stationary conditions,

$$-f_1c_1 + f_2c_2 + r_1D_1^{-1}s_1\lambda_1 + r_2D_2^{-1}s_2\lambda_2 = 0, \quad (11)$$

$$f_1s_1 - f_2s_2 + r_1D_1^{-1}c_1\lambda_1 + r_2D_2^{-1}c_2\lambda_2 = Mg, \quad (12)$$

$$R\lambda_1 - R\lambda_2 = 0. \quad (13)$$

Because we aim at controlled rolling to obtain a given object orientation through rolling motion, then Eq. (13) yields  $\lambda_1 = \lambda_2$ . Now, let  $r_1 = r_2$ ,  $k_1 = k_2 = k$ ,  $\alpha_1 = \alpha_2$  for simplicity reasonably, and thus Eqs. (11) and (12) can be satisfied for

$$f_i = \frac{1}{2}Mgs_i, \quad (14)$$

$$\lambda_i = \frac{1}{2} \frac{D_i}{r_i} Mgc_i, \quad (15)$$

for  $i = 1, 2$ . This solution satisfies (11)–(13), indicating that the object is immobilized on a manifold guaranteeing object grasping, if Eqs. (14) and (15) are fulfilled with  $\alpha_1 = \alpha_2$  at rest, i.e.,  $\dot{\nu} = 0$ . Therefore, Eqs. (14) and (15) can be considered as the desired value to achieve grasping.

## 3 Optimal grasping and control orientation

Given that deformation and contact area are usually unknown in practice, even in the well-structured environment based on the Hertz model for the lossless environment, we avoid such measurements or avoid assuming a-priori information of these parameters. The challenge now is to design a feedback controller to regulate contact and the tangential forces to achieve dynamical grasping subject to constraints (11)–(13) to guarantee object angle manipulation, under the gravity effect, and without angle measurement. Let us depart from the idea behind the optimal dynamical grasping: from an initial condition  $f_i(0)$  and  $\alpha_1 = \alpha_2$ , minimize the constraint wrench to obtain grasp with minimum effort. To achieve this, we aim at designing a controller to inject an artificial equilibrium point through controlled tangential forces. To simplify the methodology followed in our approach, firstly we present the controller for the planar case,  $g = 0$ .

### 3.1 Control design of optimal grasping without gravity

Assume without loss of generality that  $f_i = f_2 = f_d$  and  $\lambda_1 = \lambda_2 = 0$ , with  $\alpha_1 = \alpha_2$ ,  $D_1 = D_2$ ,  $r_1 = r_2$ , and  $k_1 = k_2 = k$ , and then let the joint controller be

$$\tau_i = -\mathbf{K}_{q_i} \dot{q}_i - (-1)^i F_{d_i} \mathbf{J}_i^T(q_i) \begin{bmatrix} c_i \\ -s_i \end{bmatrix} - r_i \left( D_i^{-1} \mathbf{J}_i^T(q_i) \begin{bmatrix} s_i \\ c_i \end{bmatrix} - \mathbf{e}_i \right) \lambda_{d_i} - \bar{u}_{\text{ext}} - \bar{u}_{\theta_i}, \quad (16)$$

where  $\mathbf{K}_{q_i} \in \mathbb{R}_+^{4 \times 4}$  represents the damping positive definite matrix, while  $\bar{u}_{\theta_i} \in \mathbb{R}^4$  and  $\bar{u}_{\text{ext}}$  which are the orientation input and the regulation of projection of normal forces, respectively, are defined as

$$\begin{aligned} \bar{u}_{\text{ext}} &= r_i D_i^{-1} \mathbf{J}_i^T(q_i) \begin{bmatrix} s_i \\ c_i \end{bmatrix} F_\beta, \\ \bar{u}_{\theta_i} &= (-1)^{i+1} \frac{\beta_\theta \overline{\Delta\theta}}{D_L} \mathbf{J}_i^T(q_i) \begin{bmatrix} y_1 - y_2 \\ x_2 - x_1 \end{bmatrix} \end{aligned} \quad (17)$$

with  $\beta_\theta > 0$ ,  $D_L = (x_2 - x_1)^2 + (y_1 - y_2)^2$ ,  $\overline{\Delta\theta} = \hat{\theta} - \theta_d$ , the estimation of orientation angle error with  $\hat{\theta} = \tan^{-1}(\frac{y_1 - y_2}{x_2 - x_1})$  and  $\theta_d$ , the desired object angle. To guarantee the restraint conditions on the object, with  $g = 0$ , we have that  $F_{d_i} \in \mathbb{R}$  and  $\lambda_{d_i} \in \mathbb{R}$  will be designed as

$$F_{d_i} = \frac{f_d}{2} (1 + \cos(\Delta\alpha)), \quad (18)$$

$$\lambda_{d_i} = -\frac{f_d D_i}{2 r_i} \sin(\Delta\alpha) - F_\beta, \quad (19)$$

where  $f_d \in \mathbb{R}_+$  stands for the desired contact force that assures grasp closure,  $\Delta\alpha = \alpha_1 - \alpha_2 + \theta_d$ , and  $F_\beta$  represents an induced force via  $\Delta\bar{\beta}$ . Finally,  $F_\beta$  is proposed as follows:

$$F_\beta = K_{\beta_p} \Delta\bar{\beta} + K_{\beta_v} \dot{\Delta\bar{\beta}}, \quad (20)$$

where  $K_{\beta_p}, K_{\beta_v} > 0$  are positive feedback gains, while  $\Delta\bar{\beta} = \bar{\beta} - \beta_d$  is the relative angle error between the normal forces with  $\bar{\beta} = r_1 \alpha_1 - r_2 \alpha_2 + \pi$  which is the relative (internal) angle between normal force vectors weighted by fingertip radii and  $\beta_d$  which is the desired relative angle between normal forces.

### 3.2 Closed-loop error dynamics

#### 3.2.1 Closed-loop finger error dynamics

Substituting (16) into (8), one obtains

$$\begin{aligned} \mathbf{H}_i(\mathbf{q}_i) \ddot{\mathbf{q}}_i + \mathbf{C}_i(\mathbf{q}_i, \dot{\mathbf{q}}_i) \dot{\mathbf{q}}_i - (-1)^i \Delta f_i \mathbf{J}_i^T(\mathbf{q}_i) \begin{bmatrix} c_i \\ -s_i \end{bmatrix} + \mathbf{K}_{q_i} \dot{\mathbf{q}}_i - r_i \left( \mathbf{J}_i^T(\mathbf{q}_i) D_i^{-1} \begin{bmatrix} s_i \\ c_i \end{bmatrix} - \mathbf{e}_i \right) \Delta \lambda_i \\ + r_i D_i^{-1} \mathbf{J}_i^T(\mathbf{q}_i) \begin{bmatrix} s_i \\ c_i \end{bmatrix} F_\beta + \bar{u}_{\theta_i} = \mathbf{u}_{c1}, \end{aligned} \quad (21)$$

where  $\Delta f_i = f_i - F_{d_i} \in \mathbb{R}$  and  $\Delta \lambda_i = \lambda_i - \lambda_{d_i} \in \mathbb{R}$  are the normal and tangential force errors, respectively.

#### 3.2.2 Closed-loop object error dynamics

Using (18) and (19) in (9), one obtains

$$\begin{aligned} \mathbf{H}_0 \ddot{\mathbf{p}} - \sum_{i=1}^2 \left( (-1)^i \begin{bmatrix} -c_i \\ s_i \\ 0 \end{bmatrix} \right) \Delta f_i - \sum_{i=1}^2 \left( (-1)^i R \begin{bmatrix} 0 \\ 0 \\ 1 \end{bmatrix} - r_i D_i^{-1} \begin{bmatrix} s_i \\ c_i \\ 0 \end{bmatrix} \right) \Delta \lambda_i \\ + \begin{bmatrix} -(r_1 D_1^{-1} s_1 + r_2 D_2^{-1} s_2) F_\beta \\ -(r_1 D_1^{-1} c_1 + r_2 D_2^{-1} c_2) F_\beta \\ -\frac{1}{2} R f_d D_{12} \sin(\Delta\alpha) \end{bmatrix} = 0, \end{aligned} \quad (22)$$

where  $D_{12} = \bar{r}_1^{-1} - \bar{r}_2^{-1} \in \mathbb{R}$  for  $\bar{r}_i = r_i D_i^{-1} \in \mathbb{R}$  with  $0 < \sin(\Delta\alpha) < 1$ .

#### 3.2.3 Closed-loop finger+object error dynamics

Substituting (17) into (21), the compact form of the complete error dynamics is defined as

$$\mathbf{H} \ddot{\mathbf{v}} + \mathbf{C} \dot{\mathbf{v}} + \mathbf{K} \mathbf{v} + \mathbf{A} \Delta \xi = \mathbf{u}_{cl}, \quad (23)$$

where  $\mathbf{H} = \text{diag}(\mathbf{H}_1(\mathbf{q}_1), \mathbf{H}_2(\mathbf{q}_2), \mathbf{H}_0) \in \mathbb{R}^{11 \times 11}$ ,  $\mathbf{C} = \text{diag}(\mathbf{C}_1(\mathbf{q}_1, \dot{\mathbf{q}}_1), \mathbf{C}_2(\mathbf{q}_2, \dot{\mathbf{q}}_2), \mathbf{0}_{3 \times 3}) \in \mathbb{R}^{11 \times 11}$ ,  $\mathbf{K} = \text{diag}(\mathbf{K}_{q_1}, \mathbf{K}_{q_2}, \mathbf{0}_{3 \times 3}) \in \mathbb{R}^{11 \times 11}$ ,  $\mathbf{A} = [\mathbf{A}_1, \mathbf{A}_2] \in \mathbb{R}^{11 \times 7}$  called interaction matrix (details in Appendix A),  $\Delta \xi = [\Delta f_1, \Delta f_2, \Delta \lambda_1, \Delta \lambda_2, F_\beta, \sin(\Delta\alpha), \overline{\Delta\theta}]^T \in \mathbb{R}^7$  stands for the primary control vector, and  $\mathbf{u}_{cl} \equiv 0$  is useful only for stability analysis purposes.

### 3.2.4 Stability analysis

Now, we are in conditions to state the main result.

**Proposition 1.** Consider a non-empty connected set

$$\Omega_0 = \left\{ \boldsymbol{\nu}, \dot{\boldsymbol{\nu}} : \delta_{di} = \sqrt{\frac{f_{di}}{k}} \geq 0, \{\boldsymbol{\nu}, \dot{\boldsymbol{\nu}}\} \in \mathcal{M}_{\varphi_r} \right\} \quad (24)$$

and the system (8) and (9) in closed-loop with the control law (16). For small errors on initial conditions  $\boldsymbol{\nu}(0) \in \Omega_0$ , there exists a basic constraint manifold,  $\mathcal{M}_c = \{\boldsymbol{\nu}, \dot{\boldsymbol{\nu}} : (\varphi_{r_i}, \dot{\varphi}_{r_i}, \Delta f_i, \Delta \lambda_i, \Delta \beta, \overline{\Delta \theta}) = (0, 0, 0, 0, 0, 0)\}$  such that any solution trajectory of (23) converges locally asymptotically to  $\mathcal{M}_c$  as  $t \rightarrow \infty$ . Thus, the convergence of the primary control vector  $\Delta \xi$  is guaranteed without measurements of the deformations, that is, neither contact area nor contact force of the object angle.

*Proof.* A passivity-based analysis of the closed-loop system yields, for input  $\mathbf{u}_{cl}$  and output  $\mathbf{y}_{cl} = \boldsymbol{\nu}$ ,

$$\begin{aligned} \langle \mathbf{u}_{cl}, \mathbf{y}_{cl} \rangle &= \frac{d}{dt} (K(\mathbf{q}, \dot{\boldsymbol{\nu}}) + \Delta P_E(\boldsymbol{\nu}) + P_{\text{art}}(\boldsymbol{\nu})) + \dot{\mathbf{q}}_1^T \mathbf{K}_{q_1} \dot{\mathbf{q}}_1 + \dot{\mathbf{q}}_2^T \mathbf{K}_{q_2} \dot{\mathbf{q}}_2 \\ &\quad + F_\beta \sum_{i=1}^2 r_i D_i^{-1} \left( \begin{bmatrix} \dot{x}_i & \dot{y}_i \end{bmatrix} \begin{bmatrix} s_i \\ c_i \end{bmatrix} \right) - F_\beta \left( \begin{bmatrix} \dot{x} & \dot{y} \end{bmatrix} \begin{bmatrix} \bar{r}_1 s_1 + \bar{r}_2 s_2 \\ \bar{r}_1 c_1 + \bar{r}_2 c_2 \end{bmatrix} \right) - \dot{\theta} R f_d \frac{1}{2} D_{12} C S \\ &= \frac{d}{dt} (K(\mathbf{q}, \dot{\boldsymbol{\nu}}) + \Delta P_E(\boldsymbol{\nu}) + P_{\text{art}}(\boldsymbol{\nu})) + \dot{\mathbf{q}}_1^T \mathbf{K}_{q_1} \dot{\mathbf{q}}_1 + \dot{\mathbf{q}}_2^T \mathbf{K}_{q_2} \dot{\mathbf{q}}_2 + \dot{\beta} F_\beta - \dot{\theta} \left( R \frac{f_d}{2} D_{12} \sin(\Delta \alpha) \right) \\ &= \frac{d}{dt} \bar{E}(\boldsymbol{\nu}, \dot{\boldsymbol{\nu}}) + \dot{\mathbf{q}}^T \mathbf{K}_q \dot{\mathbf{q}} + K_{\beta v} \dot{\beta}^2 - \dot{\theta} \left( R \frac{f_d}{2} D_{12} \sin(\Delta \alpha) \right), \end{aligned} \quad (25)$$

where  $\mathbf{K}_q = \text{diag}(\mathbf{K}_{q_1}, \mathbf{K}_{q_2})$ ,  $\bar{E}(\boldsymbol{\nu}, \dot{\boldsymbol{\nu}}) = K(\mathbf{q}, \dot{\boldsymbol{\nu}}) + \Delta P_E(\boldsymbol{\nu}) + P_{F_\beta} + P_{\text{art}} > 0$  represents the closed-loop storage energy function of error system,  $\Delta P_E(\boldsymbol{\nu}) \in \mathbb{R}$  stands for the elastic potential energy error of the system,  $P_{F_\beta} = \frac{1}{2} K_{\beta p} \Delta \bar{\beta}^2$  represents the artificial potential energy to induce the optimal grasping condition, while  $P_{\text{art}} = \frac{\beta_0}{2} \overline{\Delta \theta}^2$  is the potential used to induce an equilibrium point to the desired object angle. Now, assuming that  $r_1 = r_2$ , without loss of generality, we have that  $D_{12} = \frac{R(r_2 - r_1) + \delta_2 r_1 - \delta_1 r_2}{r_1 r_2} \leq 1$ , such that  $|\dot{\theta}|(\gamma D_{12} \sin(\Delta \alpha)) \leq |\dot{\theta}| \epsilon_1$  with  $\gamma = R \frac{f_d}{2} \in \mathbb{R}$  and  $\epsilon_1 > 0$ . Then, with  $\mathbf{u}_{cl} = 0$ , we have that Eq. (25) can be expressed as

$$\dot{\bar{E}}(\boldsymbol{\nu}, \dot{\boldsymbol{\nu}}) \leq -\dot{\mathbf{q}}^T \mathbf{K}_q \dot{\mathbf{q}} - K_{\beta v} \dot{\beta}^2 + |\dot{\theta}| \epsilon_1. \quad (26)$$

Notice that  $\dot{\bar{E}}(\boldsymbol{\nu}, \dot{\boldsymbol{\nu}})$  is not a Lyapunov function in the primary constrained manifold, but certainly  $\dot{\bar{E}}(\boldsymbol{\nu}, \dot{\boldsymbol{\nu}})$  can be used to analyse the convergence properties of the autonomous system (23) on the largest invariant set. Applying the maximum invariance set to (26) for the origin at  $\boldsymbol{\nu} = 0$  leads to trivial annihilator when  $\dot{\boldsymbol{\nu}} = (0, 0, 0)$  given that  $\bar{\beta}$  is a function of  $\dot{x}$  and  $\dot{y}$ . Thus,  $\dot{\bar{E}}(\boldsymbol{\nu}, \dot{\boldsymbol{\nu}}) = 0$  implies that  $\dot{\boldsymbol{\nu}} = 0$ . This means that for small initial conditions  $\boldsymbol{\nu}(0) \in \Omega_0$  and large enough joint damping gains  $\mathbf{K}_q$ , we have that  $\dot{\bar{E}}(\boldsymbol{\nu}, \dot{\boldsymbol{\nu}})$  becomes negative semi-definite along the solution trajectories with equilibrium at  $\dot{\boldsymbol{\nu}} = 0 \implies \dot{\boldsymbol{\nu}} = 0$ . Since the desired trajectories are constant, the closed-loop system is autonomous, which leads us to conclude that the largest invariant set  $\dot{\bar{E}}(\boldsymbol{\nu}, \dot{\boldsymbol{\nu}}) = 0 \implies \dot{\boldsymbol{\nu}} = 0$  and consequently  $\dot{\boldsymbol{\nu}} = 0$ , and then Eq. (23) becomes

$$\mathbf{A} \Delta \xi = 0. \quad (27)$$

Thus, there exists a unique critical point that satisfies (27) only if the matrix  $\mathbf{A}$  is full column rank. This means that if  $\Delta \xi \rightarrow 0$  then  $\Delta f_i \rightarrow 0$ ,  $\Delta \lambda_i \rightarrow 0$ ,  $F_\beta \rightarrow 0$ ,  $\sin(\Delta \alpha) \rightarrow 0$  and  $\overline{\Delta \theta} \rightarrow 0$ .

**Remark 4.** Precise conditions for optimal grasping are encoded through  $\beta_d$ , at the expense of slow convergence rate not only because of high damping but because stability is derived in the realm of stability-in-the-manifold, where attractors arise once velocity tends to zero, as is shown in the proof.

**Remark 5.** Angle convergence is achieved through indirect injection of  $\lambda_i$  through the underactuated object dynamics structure. Overall, it is expected, intuitively and theoretically, slow convergence rate toward the basic manifold, as if mimicking a robot learning from scratch to pinch optimally an object.

**Remark 6.** A direct extension of this approach, taking into account gravity force, can be obtained by extending [44],

$$F_{d_i} = \frac{f_d}{2} (1 + \cos(\Delta\alpha)) - (-1)^i \frac{1}{2} M g s_i, \quad (28)$$

$$\lambda_{d_i} = -\frac{f_d}{2} \frac{D_i}{r_i} \sin(\Delta\alpha) + \frac{1}{2} D_i r_i^{-1} M g c_i - F_\beta. \quad (29)$$

Stability conditions are mutatis-mutandis and follow straightforward.

**Remark 7.** We can extend our proposal by considering a control structure that resembles synergies [7, 22], to account for optimal grasping, pose control, position, and orientation of the object as follows:

$$\boldsymbol{\tau}_i = -\mathbf{K}_{q_i} \dot{\mathbf{q}}_i + g_i(q_i) + \bar{u}_f + \bar{u}_t - \bar{u}_{\theta_i} + \bar{u}_{x_i} + \bar{u}_{y_i}, \quad (30)$$

where

$$\begin{aligned} \bar{u}_f &= -(-1)^i F_{d_i} \mathbf{J}_i^T(\mathbf{q}_i) \begin{bmatrix} c_i \\ -s_i \end{bmatrix} - r_i \left( D_i^{-1} \mathbf{J}_i^T(\mathbf{q}_i) \begin{bmatrix} s_i \\ c_i \end{bmatrix} - \mathbf{e}_i \right) \lambda_{d_i}, \\ \bar{u}_t &= -r_i D_i^{-1} \mathbf{J}_i^T(\mathbf{q}_i) \begin{bmatrix} s_i \\ c_i \end{bmatrix} F_\beta, \\ \bar{u}_{x_i} &= -\frac{\gamma_x}{2} (\bar{x} - x_d) \frac{\partial x_i}{\partial q_i}, \quad \bar{u}_{y_i} = -\frac{\gamma_y}{2} (\bar{y} - y_d) \frac{\partial y_i}{\partial q_i}, \end{aligned}$$

for  $\gamma_x > 0$ ,  $\gamma_y > 0$ , desired object positions are given by  $(x_d, y_d)$ , while  $\bar{x}$ ,  $\bar{y}$  are the estimated object positions with  $\bar{x} = \frac{x_1 + x_2}{2}$  and  $\bar{y} = \frac{y_1 + y_2}{2}$  for  $x_i, y_i$ , the center of the  $i$ -th fingertip.

**Remark 8.** If dynamics of the  $i$ -th finger is subject to friction at contact, then Eq. (8) can be written as

$$\mathbf{H}_i(\mathbf{q}_i) \ddot{\mathbf{q}}_i + \mathbf{C}_i(\mathbf{q}_i, \dot{\mathbf{q}}_i) \dot{\mathbf{q}}_i + g_i(\mathbf{q}_i) = \boldsymbol{\tau}_i - \boldsymbol{\tau}_F + (-1)^i f_i \mathbf{J}_i^T(\mathbf{q}_i) \begin{bmatrix} c_i \\ -s_i \end{bmatrix} + r_i \left( \mathbf{J}_i^T(\mathbf{q}_i) D_i^{-1} \begin{bmatrix} s_i \\ c_i \end{bmatrix} - \mathbf{e}_i \right) \lambda_i,$$

where  $\boldsymbol{\tau}_F = \mathbf{B}_c \dot{\mathbf{q}}_i + \mathbf{C} \tanh(D \dot{\mathbf{q}}_i)$  represents viscosity and an approximated Coulomb friction at contact, respectively, with  $\mathbf{B}_c$  and  $\mathbf{C}$  being diagonal positive definite matrices and  $\tanh(D \dot{\mathbf{q}}_i)$  being a reasonable approximation of the non-smooth Coulomb friction model with  $D \in \mathbb{R}_+^{n \times n}$ . Using  $\boldsymbol{\tau}_i$  defined in (30), the closed-loop is defined as

$$\begin{aligned} \mathbf{H}_i(\mathbf{q}_i) \ddot{\mathbf{q}}_i + \mathbf{C}_i(\mathbf{q}_i, \dot{\mathbf{q}}_i) \dot{\mathbf{q}}_i - (-1)^i \Delta f_i \mathbf{J}_i^T(\mathbf{q}_i) \begin{bmatrix} c_i \\ -s_i \end{bmatrix} + \bar{\mathbf{K}} \dot{\mathbf{q}}_i + \mathbf{C} \tanh(D \dot{\mathbf{q}}_i) \\ - r_i \left( \mathbf{J}_i^T(\mathbf{q}_i) D_i^{-1} \begin{bmatrix} s_i \\ c_i \end{bmatrix} - \mathbf{e}_i \right) \Delta \lambda_i + r_i D_i^{-1} \mathbf{J}_i^T(\mathbf{q}_i) \begin{bmatrix} s_i \\ c_i \end{bmatrix} F_\beta + \bar{u}_{\theta_i} = u_{c1}, \end{aligned}$$

where  $\bar{\mathbf{K}} = \mathbf{K}_{q_i} + \mathbf{B}_c$ . Following similar steps of Subsection 3.2, it is possibly guaranteed that there exists a critical point that satisfies (27) only if matrix  $\mathbf{A}$  is full column rank. In this condition  $\Delta f_i \rightarrow 0$ ,  $\Delta \lambda_i \rightarrow 0$ ,  $F_\beta \rightarrow 0$ ,  $\sin(\Delta\alpha) \rightarrow 0$  and  $\Delta\theta \rightarrow 0$ .

**Remark 9.** Let friction cone be considered at contact as the set wrenches that satisfies the classical Coulomb's law at contact. Then  $|f_t| \leq \mu |f_n|$  where  $|f_t|$  and  $|f_n|$  stand for the tangential and normal components of the contact force, for the Coulomb coefficient  $\mu > 0$  [47]. Notice that, from (18) and (19), such friction cone is implicitly assumed and satisfied since  $|\lambda_{d_i}| \leq \lambda_{\max} = \mu |F_d|$  is satisfied with  $F_d > 0$ .

## 4 Numerical simulations

### 4.1 The simulator and system parameters

The simulator is programmed in Matlab R2017a, based on a variation of the Bogacki-Shampine variable-step stiff numerical integrator [48], implemented as ode23tb with variable step, and an absolute error

**Table 1** Physical parameters of the robotic fingers

Parameter	Value (m)	Parameter	Value
$L_{i1}$	0.1	$M_{i1}$	0.5 kg
$L_{i2}$	0.08	$M_{i2}$	0.3 kg
$L_{i3}$	0.06	$M_{i3}$	0.15 kg
$L_{i4}$	0.03	$M_{i4}$	0.1 kg
$l_{cm_{i1}}$	0.045	$I_{i1}$	$6.5 \times 10^{-4}$ kg·m <sup>2</sup>
$l_{cm_{i2}}$	0.035	$I_{i2}$	$2.5 \times 10^{-4}$ kg·m <sup>2</sup>
$l_{cm_{i3}}$	0.025	$I_{i3}$	$5 \times 10^{-5}$ kg·m <sup>2</sup>
$l_{cm_{i4}}$	0.01	$I_{i4}$	$2 \times 10^{-6}$ kg·m <sup>2</sup>

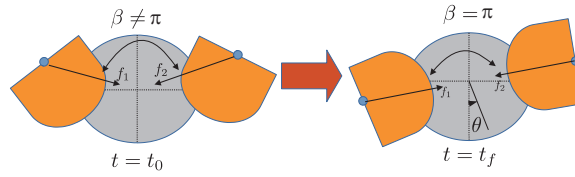


**Figure 4** (Color online) The optimal grasping of a circular object [44].

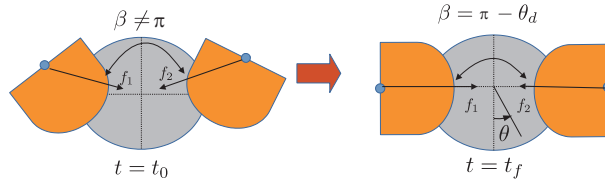


**Figure 5** (Color online) Proposed optimal grasping and orientation control of a circular object with  $\theta_d = 0$  rad.

tolerance of  $1 \times 10^{-4}$  m. A constrained stabilization method (CSM) [49], is introduced for numerical stabilization of the DAE-2 system, whose initial conditions for the overall system are consistent at  $t = t_0$  as the initial grasp for  $f_i(0) > 0, i = 1, 2$ .

Physical parameters of robotic fingers are described in Table 1 where  $L_{ij}, l_{cm_{ij}}, M_{ij}$  and  $I_{ij}$  stand for the  $j$ -th link’s length, distance to center of mass, mass, and mass moment of inertia, of the  $i$ -th robotic finger, respectively. Additionally,  $M = 0.1$  kg,  $I = 2 \times 10^{-3}$  kg·m<sup>2</sup> and  $R = 0.05$  m represent the mass, mass moment of inertia and radius of the object, respectively. Finally, the  $i$ -th semi-hemispherical soft-fingertip has a stiffness parameter of  $k_i = 10000$  kg·m/s<sup>2</sup>m<sup>2</sup> with  $r_i = 0.02$  m of radius.

In this section two set numerical simulation results are presented. The first one set shows the performance of two robotic fingers with soft tips to reach the optimal grasping condition manipulating a circular object; see Figure 4. In the second set, the simulation results of optimal grasping and orientation control of a circular object avoiding the measure of the object angle are presented; see Figure 5.

## 4.2 Simulation results

The system is initialized with  $\mathbf{q}_1(0) = [0.75, 1, 0.65, 0.2]^T$  rad,  $\mathbf{q}_2(0) = [0.85, 0.8, 0.8, 0.2]^T$  rad,  $\bar{\mathbf{p}}(0) = [0.075, 0.21]^T$  m and  $\theta(0) = 0.0$  rad, which give rise to  $\alpha_1(\mathbf{q}_1(0), \bar{\mathbf{p}}(0)) = -0.0351$  rad,  $\alpha_2(\mathbf{q}_2(0), \bar{\mathbf{p}}(0)) = -0.1109$  rad. The initial velocities of the system are all zero, that is,  $\dot{\mathbf{q}}_1(0) = \dot{\mathbf{q}}_2(0) = [0, 0, 0, 0]^T$  rad/s  $\dot{\bar{\mathbf{p}}}(0) = [0, 0]^T$  m/s, and  $\dot{\theta}(0) = 0$  rad/s. The feedback control gains are given as  $\mathbf{K}_{q_i} = \text{diag}(0.05)$  kg·m<sup>2</sup>/s,  $K_{\beta_p} = 20$  kg·m/s<sup>2</sup>,  $K_{\beta_v} = 8$  kg/s. The desired values to achieve optimal grasping are defined as  $f_d = 2.5$  N and  $\beta_d = \pi - \theta_d$  rad.

### 4.2.1 Dynamical optimal grasping

To achieve optimal grasping of a circular rigid object by two robotic fingers with soft tips, we assume that  $\bar{u}_{\theta_i} = 0$  in (16). Figure 6 shows that contact and tangential forces converge to the desired values in a few seconds. In special, the tangential forces converge a bit later than the contact forces, which represents the necessary time to reach the optimal grasping conditions,  $\alpha_1 = \alpha_2$ . Given that the induced forces to get the optimal grasping conditions are conducting through the tangential forces, changes in the position and orientation of the object are presented; see Figure 7.

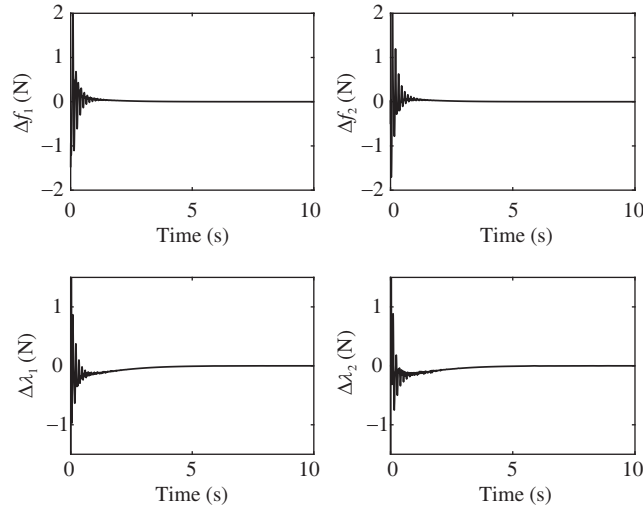


**Figure 6** Optimal grasping with  $\beta_d = \pi$ .

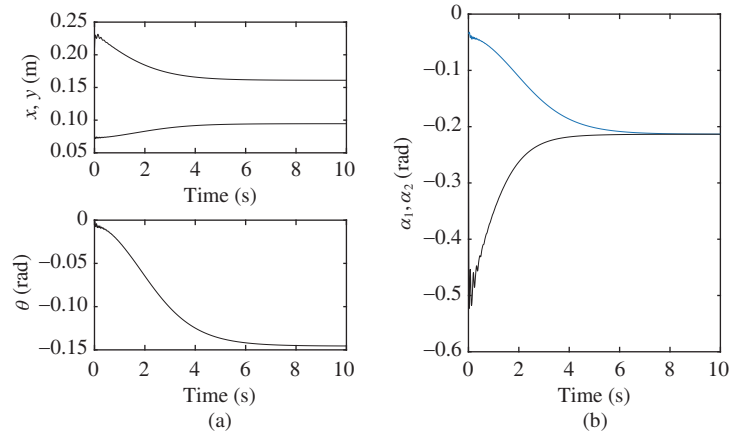


**Figure 7** (Color online) Optimal grasping: (a) CoM<sub>o</sub> and the object angle  $\theta$ , (b) internal angles  $\alpha_i$ , for  $i = 1, 2$ .

#### 4.2.2 Optimal grasping and orientation control

In this simulation, assume that the desired orientation is defined as  $\theta_d = 0$  rad with  $\beta_\theta = 0.5$  kg·m/s. As in the previous simulation, we notice the fast convergence of contact and tangential forces; see Figure 8. However, contrary to the previous simulation, we notice that one of the internal angles quickly reaches the zero value while the other angle tends toward zero exponentially; see Figure 9(b). Thus, only one of the soft tips, through the rolling motion, is used to guarantee the optimal grasping condition avoiding any object information. In Figure 9(c) the exponential performance of  $\overline{\Delta\theta}$  is shown.

Given that the value of the object angle orientation is calculated on relations between the center positions of the soft fingertips, we have that  $\hat{\theta}$  is not equal to the real value of  $\theta$ . This explains the value of  $\theta$  in Figure 9. The finger performance can be compared to in-hand manipulation skills required to do a simple rotation, and turn an object through the pads of the thumb and index fingers.

As a final set of simulations, we present a comparative study between the proposed approach and [43], where it is assumed that the object angle is available. The simulation conditions are defined as  $q_1(0) = [0.55, 1.1, 1.4, 0.12]^T$  rad,  $q_2(0) = [0.60, 1.1, 1.05, 0.5]^T$  rad;  $\bar{p}(0) = [0.075, 0.155]^T$  m and  $\theta(0) = 0.2$  rad with  $f_d = 2.5$  N and  $\theta_d = 0$  rad; see Figure 10. We notice in Figure 10(b) that convergence to zero of the internal angles is reached in few seconds, and thus the convergence of  $\overline{\Delta\theta}$  is reached rapidly. Using [43], unlike the proposed approach, the convergence of internal angles is slower such that the convergence of  $\overline{\Delta\theta}$  is slow, too; see Figure 10(b).

Finally, in Figures 11 and 12 we show the optimal grasping and orientation control of the circular object for  $\theta_d = -0.2$  rad. As in the previous case, we can notice the convergence of  $\Delta f_i$  and  $\Delta \lambda_i$  is before that of  $\overline{\Delta\theta}$ . For this simulation we assume that  $q_1(0) = [0.2, 1.7, 0.8, 0.3]^T$  rad,  $q_2(0) = [0.2, 1.7, 0.8, 0.3]^T$

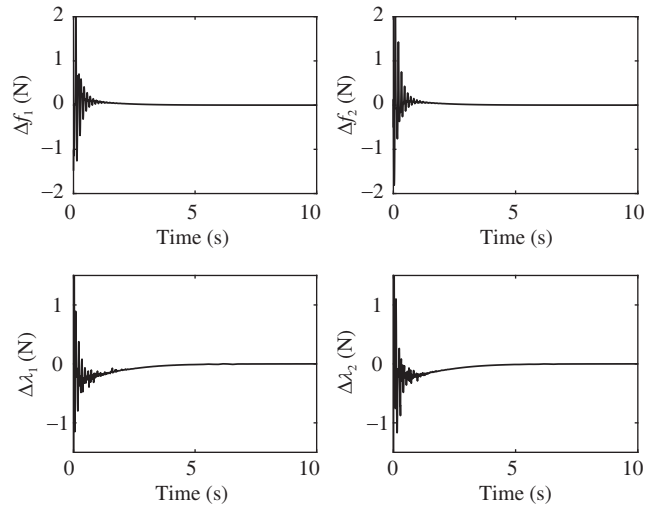


**Figure 8** Optimal grasping and orientation control with  $\beta_d = \pi - \theta_d$ .

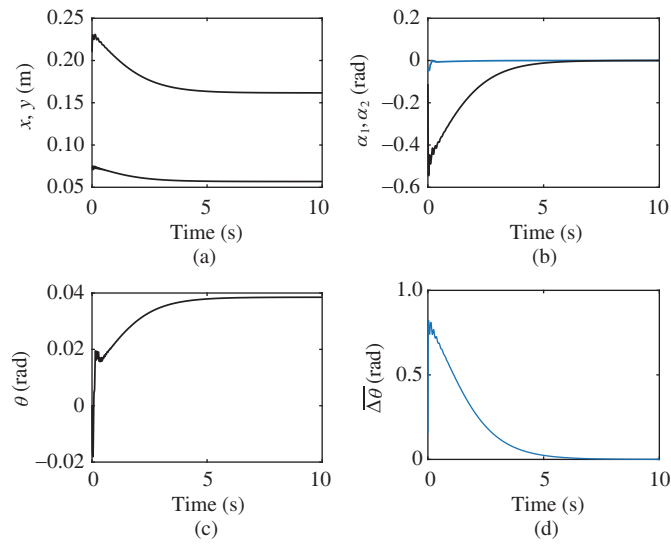


**Figure 9** (Color online) Optimal grasping and orientation control: (a) CoM<sub>o</sub>, (b) internal angles  $\alpha_i$ , (c) the object angle  $\theta$ , (d) orientation angle error  $\Delta\theta$ .

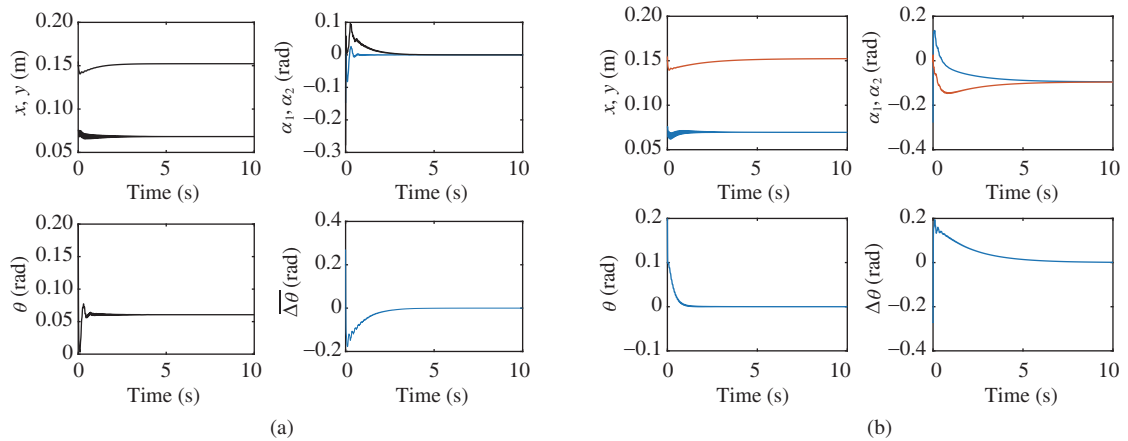


**Figure 10** (Color online) Comparative study between the proposed approach and [43]: object coordinates, internal angles and error angles. (a) Without object angle measurement; (b) with object angle measurement.

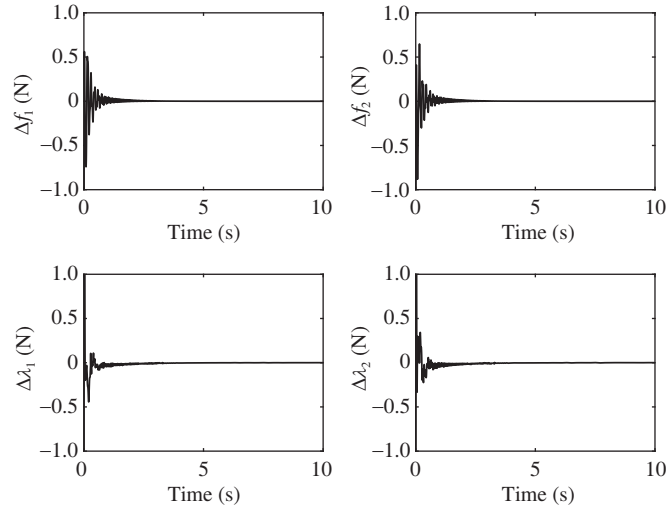


**Figure 11** Optimal grasping and orientation control with  $\beta_d = \pi - \theta_d$  and  $\theta_d = -0.2$  rad.

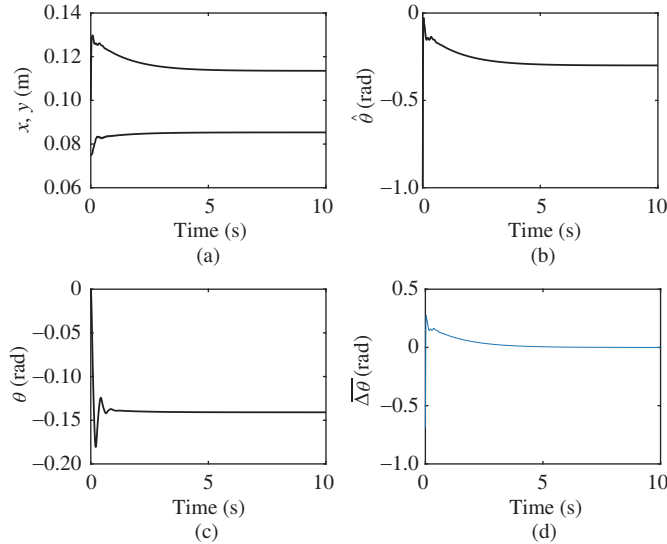


**Figure 12** (Color online) Optimal grasping and orientation control with  $\theta_d = -0.2$  rad: (a) CoM<sub>*x, y*</sub>, (b)  $\dot{\theta}$ , (c) the object angle  $\theta$ , (d) orientation angle error  $\Delta\theta$ .

rad,  $\bar{p}(0) = [0.075, 0.10]^T$  m and  $\theta(0) = 0.2$  rad with  $f_d = 2.5$  N.

#### 4.2.3 Optimal grasping and orientation control under gravity effect

In this subsection we present the simulation results of optimal grasping of a circular object under the gravity effect. For this case, assume that  $F_{d_i}$  and  $\lambda_{d_i}$  are defined as in (28) and (29), respectively, while the control law is defined by (30) with  $\bar{u}_{x_i} = 0$  and  $\bar{u}_{y_i} = 0$ .

For the first simulation we consider that  $\bar{p}(0) = [0.15, 0.2]^T$  m and  $\theta(0) = 0.0$  rad with  $f_d = 2.5$  N and  $\theta_d = 0$  rad; see Figure 13. Finally for the second simulation we consider that  $\bar{p}(0) = [0.075, 0.155]^T$  m and  $\theta(0) = 0.0$  rad with  $f_d = 2.5$  N and  $\theta_d = 0.2$  rad; see Figure 14. In both simulations, we notice that there is a transition period in the first few seconds where the controller tries to compensate the gravity force. As in previous simulations,  $\Delta\theta$  has an exponential convergence in a few seconds after that the contact force error and tangential force errors have converged.

To debug and test the proposed algorithm a V-REP and Matlab co-simulation is presented. The design of the robotic fingers is based on dimensions of Dynamixel servos; see Figure 15. The new physical parameters are defined as  $L_{i1} = 0.088$  m,  $L_{i2} = 0.088$  m,  $L_{i3} = 0.036$  m,  $M_{i1} = 0.2$ ,  $M_{i2} = 0.2$  kg,  $M_{i3} = 0.15$  kg,  $l_{cm_{i1}} = 0.06$  m,  $l_{cm_{i2}} = 0.06$  m and  $l_{cm_{i3}} = 0.025$  m for the  $i$ -th robotic finger. Additionally,  $M = 0.04$  kg and  $R = 0.05$  m are the mass and radius of the object, respectively. Finally,

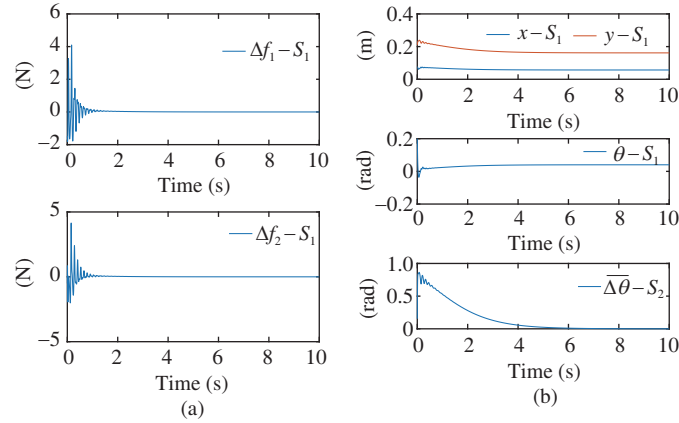


**Figure 13** (Color online) Optimal grasping under gravity effect: performance of the  $\Delta f_i$  and the object coordinates,  $i = 1, 2$ , where  $\bar{p}(0) = [0.15, 0.2]^T$  m and  $\theta(0) = 0.0$  rad with  $f_d = 2.5$  N and  $\theta_d = 0$  rad. (a) Contact force error; (b) object coordinates.

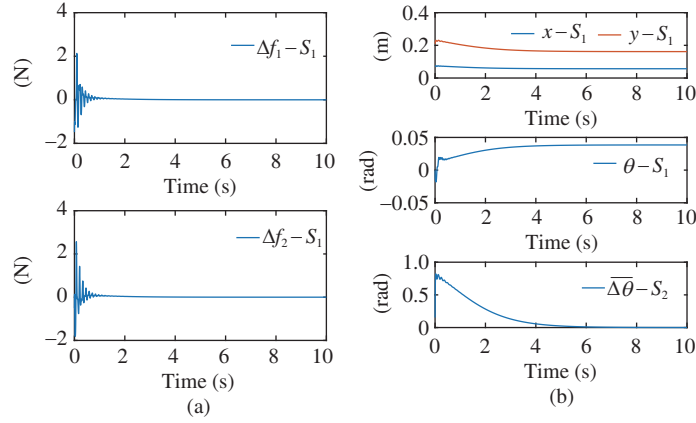


**Figure 14** (Color online) Optimal grasping under gravity effect: performance of the  $\Delta f_i$  and the object coordinates,  $i = 1, 2$ , where  $\bar{p}(0) = [0.075, 0.155]^T$  m and  $\theta(0) = 0.0$  rad with  $f_d = 2.5$  N and  $\theta_d = 0.2$  rad. (a) Contact force error; (b) object coordinates.

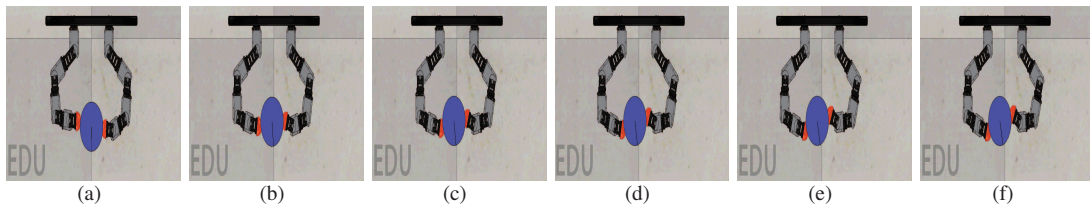


**Figure 15** (Color online) Performance of the stable grasping and orientation of a circular object avoiding any object information: (a)  $t = 0$  s, (b)  $t = 5$  s, (c)  $t = 10$  s, (d)  $t = 15$  s, (e)  $t = 20$  s. (f)  $t = 25$  s.

the  $i$ -th hemispherical soft-fingertip has a stiffness parameter of  $k_i = 270563.4$  kg·m/s<sup>2</sup>·m<sup>2</sup>, with radius  $r_i = 0.03$  m and  $L_0 = 0.20$  m being the distance between each finger's base.

For this simulation we consider that initial conditions are given as  $\mathbf{q}_1(0) = [1.21798, 0.535359, 1.97116]^T$  rad,  $\mathbf{q}_2(0) = [1.29621, 0.61666, 1.96196]^T$  rad and  $\dot{\mathbf{q}}_1(0) = \dot{\mathbf{q}}_2(0) = [0, 0, 0]^T$  rad/s for fingers and  $\bar{p}(0) = [0.0889231, 0.114769]^T$  m,  $\theta(0) = 0$  rad and  $\dot{\bar{p}}(0) = [0, 0]^T$  m/s,  $\dot{\theta}(0) = 0$  rad/s for the object.

To render simulation data from Matlab, these are stored in a data file, and then loaded into the physical simulation engine V-REP. Figure 15(a) renders the fingers in contact to the object. Once grasp is achieved, fingers hold the object firmly as shown in Figure 15(b), subsequently the manipulation stage is achieved in Figures 15(c)–(e), until eventually object reaches the desired orientation in Figure 15(f). This latter figure shows how the estimation of orientation angle, indicated by a dark line in Figure 15 on the object, converges asymptotically to the desired object angle.

## 5 Conclusion

**Concluding remarks.** A circular object's reposition via two fingers with hemispherical and soft tips through optimal grasping without object angle measurement is proposed. Fundamentally, our proposal aims at understanding dexterous manipulation from an (energy) passivity perspective using SD-fingers for curved objects. The object manipulation with an arbitrary shape is feasible, assuming a local circular approximation at contact to correctly model the resulting moments concerning the CoM<sub>o</sub>. The proposed regulator provides dexterous manipulation with a skill unmatched by conventional CP-based robotic hands. It controls explicitly tangent forces, in contrast to CP wherein not such a force is modelled.

**Perspectives.** In robotics, it is customary to conduct experiments once an emergent scheme is proposed, particularly when it is claimed that dominant nonlinear constrained dynamics is considered in closed-loop with a novel controller. Experimental testing will provide evidence about the proposed approach for a particular robotic technology, then suggesting the validity of the hypothesis, and therefore the advance based the scientific method. To conduct such experiments in a real testbed, it stands for an endeavor itself to carefully verify all conditions and tuning, as well integration of fingers and object sensors, finger actuators, and processing at a unique clock thread of all low-level decision making actions.

Experiments are underway to test its performance in a laboratory testbed, similar to the render of Figure 15 based on Matlab co-simulation under RT Workshop machine, HD webcam, and Dynamixel RMX-64R servos in torque mode. The assessment of such experimental data is a challenge that requires additional settings to provide insight specific aspects of multi-robotic systems manipulating underactuated inertial objects.

### References

- Bicchi A. Hands for dexterous manipulation and robust grasping: a difficult road toward simplicity. *IEEE Trans Robot Automat*, 2000, 16: 652–662
- Mattar E. A survey of bio-inspired robotics hands implementation: new directions in dexterous manipulation. *Robot Autonomous Syst*, 2013, 61: 517–544
- Salisbury J-K. Kinematics and force analysis of articulated hands. Dissertation for Ph.D. Degree. Stanford: Stanford University, 1982
- Cole A B A, Hauser J E, Sastry S S. Kinematics and control of multifingered hands with rolling contact. *IEEE Trans Automat Contr*, 1989, 34: 398–404
- Murray R, Li Z X, Sastry S S. *A Mathematical Introduction to Robotic Manipulation*. Boca Raton: CRC Press, 1994
- Parra-Vega V, Rodríguez-Angeles A, Arimoto S, et al. High precision constrained grasping with cooperative adaptive hand-control. *J Intell Robot Syst*, 2001, 32: 235–254
- Bicchi A, Gabbicini M, Santello M. Modelling natural and artificial hands with synergies. *Phil Trans R Soc B*, 2011, 366: 3153–3161
- Stramigioli S. Modeling and IPC control of interactive mechanical systems — a coordinate-free approach. In: *Lecture Notes in Control and Information Sciences*. Berlin: Springer, 2003
- Karayiannidis Y, Doulgeri Z. Adaptive control of robot contact tasks with on-line learning of planar surfaces. *Automatica*, 2009, 45: 2374–2382
- Karayiannidis Y, Rovithakis G, Doulgeri Z. Force/position tracking for a robotic manipulator in compliant contact with a surface using neuro-adaptive control. *Automatica*, 2007, 43: 1281–1288
- Fasoulas J, Sfakiotakis M. Modeling and control for object manipulation by a two d.o.f. robotic hand with soft fingertips. *IFAC Proc Vol*, 2012, 45: 259–264
- Jia Y-B. Grasping curved objects through rolling. In: *Proceedings of IEEE International Conference on Robotics and Automation*, 2000. 377–382
- Harada K, Kaneko M. Rolling based manipulation under neighborhood equilibrium, robotics and automation. In: *Proceedings of IEEE International Conference on Robotics and Automation*, 2001. 2492–2498
- Ito S, Mizukoshi Y, Sasaki M. Numerical analysis for optimal posture of circular object grasped with frictions. In: *Proceedings of IEEE/RSJ International Conference on Intelligent Robots and Systems*, 2007. 1545–1550
- Nakashima A, Nagase K, Hayakawa Y. Simultaneous control of grasping/manipulation and contact points with rolling contact. In: *Proceedings of the 16th IFAC World Congress*, 2005
- Song S K, Park J B, Choi Y H. Dual-fingered stable grasping control for an optimal force angle. *IEEE Trans Robot*, 2012, 28: 256–262
- Marigo A, Bicchi A. Rolling bodies with regular surface: controllability theory and applications. *IEEE Trans Automat Contr*, 2000, 45: 1586–1599
- Morio Y, Arimoto S, Bae J-H. Blind grasp and manipulation of a rigid object by a pair of robot fingers with soft tips. In: *Proceedings of IEEE International Conference on Robotics and Automation*, 2007. 4707–4714
- Akella P, Cutkosky M. Manipulating with soft fingers: modeling contacts and dynamics. In: *Proceedings of International Conference on Robotics and Automation*, 1989. 767–769
- Arimoto S, Nguyen P T A, Han H Y, et al. Dynamics and control of a set of dual fingers with soft tips. *Robotica*, 2000, 18: 71–80
- Arimoto S. *Control Theory of Multi-fingered Hands*. Berlin: Springer, 2008
- Latash M L, Zatsiorsky V. Principle of superposition in human prehension. In: *Advances in Robot Control: From Everyday Physics to Human-Like Movements*. Berlin: Springer, 2006. 249–261
- Santello M, Bianchi M, Gabbicini M, et al. Towards a synergy framework across neuroscience and robotics: lessons learned and open questions. Reply to comments on: “Hand synergies: Integration of robotics and neuroscience for understanding the

control of biological and artificial hands". *Phys Life Rev*, 2016, 17: 54–60

24 Shibata M, Hirai S. Stability and graspability analysis in grasping task taking fingertip dynamics into consideration. In: Proceedings of the 2004 IEEE/RSJ International Conference on Intelligent Robots and Systems, 2004. 3686–3691

25 Inoue T, Hirai S. Why humans can manipulate objects despite a time delay in the nervous system. In: *The Human Hand as an Inspiration for Robot Hand Development*. Cham: Springer, 2014

26 Wimboeck T, Ott C, Hirzinger G G. Passivity-based object-level impedance control for a multifingered hand. In: Proceedings of IEEE/RSJ International Conference on Intelligent Robots and Systems, 2006. 4621–4627

27 Ozawa R, Arimoto S, Nguyen P T A, et al. Manipulation of a circular object in a horizontal plane by two finger robots. In: Proceedings of IEEE International Conference on Robotics and Biomimetics, 2004. 517–522

28 Nguyen P T A, Ozawa R, Arimoto S. Manipulation of a circular object by a pair of multi-DOF robotic fingers. In: Proceedings of IEEE/RSJ International Conference on Intelligent Robots and Systems, 2006. 5669–5674

29 Ozawa R, Arimoto S, Nguyen P T A, et al. Manipulation of a circular object without object information. In: Proceedings of International Conference on Intelligent Robots and Systems, 2005. 1832–1838

30 Grammatikopoulou M, Psomopoulou E, Droukas L, et al. A controller for stable grasping and desired finger shaping without contact sensing. In: Proceedings of IEEE International Conference on Robotics and Automation (ICRA), 2014. 3662–3668

31 Psomopoulou E, Karashima D, Dougeri Z, et al. Stable pinching by controlling finger relative orientation of robotic fingers with rolling soft tips. *Robotica*, 2018, 36: 204–224

32 Nakashima A, Shibata T, Hayakawa Y. Grasp and manipulation by soft finger with 3-dimensional deformation. In: Proceedings of SPIE, 2008. 6794

33 Roa M A, Suárez R. Grasp quality measures: review and performance. *Auton Robot*, 2015, 38: 65–88

34 Coelho J A, Grupen R A. Optimal multifingered grasp synthesis. In: Proceedings of the 1994 IEEE International Conference on Robotics and Automation, 1994. 1937–1942

35 Wen S Q, Wu T J. Computation for maximum stable grasping in dynamic force distribution. *J Intell Robot Syst*, 2012, 68: 225–243

36 Kim B, Oh S, Yi B, et al. Optimal grasping based on non-dimensionalized performance indices. In: Proceedings of IEEE/RSJ International Conference on Intelligent Robots and Systems, 2001. 949–956

37 Harada K, Tsuji T, Uto S, et al. Stability of soft-finger grasp under gravity. In: Proceedings of IEEE International Conference on Robotics and Automation (ICRA). 2014. 883–888

38 Shibata M, Hirai S. Stability and graspability analysis in grasping task taking fingertip dynamics into consideration. In: Proceedings of IEEE/RSJ International Conference on Intelligent Robots and Systems, 2004. 3686–3691

39 Assaf T, Roke C, Rossiter J, et al. Seeing by touch: evaluation of a soft biologically-inspired artificial fingertip in real-time active touch. *Sensors*, 2014, 14: 2561–2577

40 Ascari L, Bertocchi U, Corradi P, et al. Bio-inspired grasp control in a robotic hand with massive sensorial input. *Biol Cybern*, 2009, 100: 109–128

41 Dang H, Allen P K. Stable grasping under pose uncertainty using tactile feedback. *Auton Robot*, 2014, 36: 309–330

42 Iberall T, Bingham G, Arbib M A. Opposition space as a structuring concept for the analysis of skilled hand movements. In: *Experimental Brain Research Series 15 — Generation and Modulation of Action Patterns*. Berlin: Springer-Verlag, 1986. 158–173

43 Garcia-Rodriguez R, Villalva-Lucio M, Parra-Vega V. Dexterous dynamic optimal grasping of a circular object with pose regulation using redundant robotic soft-fingertips. In: Proceedings of 2015 IEEE/RSJ International Conference on Intelligent Robots and Systems (IROS), 2015. 6231–6237

44 Garcia-Rodríguez R, Villalva-Lucio M, Parra-Vega V. Dexterous dynamic optimal grasping of a circular object subject to gravity with soft-fingertips. *IFAC-PapersOnLine*, 2015, 48: 220–225

45 Amodio P, Mazzia F. Numerical solution of differential algebraic equations and computation of consistent initial/boundary conditions. *J Comput Appl Math*, 1997, 87: 135–146

46 Napier J, Tuttle R H, Russell H. *Hands*. Princeton: Princeton University Press, 1993

47 Mason M T. *Mechanics of Robotic Manipulation*. Cambridge: MIT Press, 2001

48 Bogacki P, Shampine L F. A 3(2) pair of Runge-Kutta formulas. *Appl Math Lett*, 1989, 2: 321–325

49 Baumgarte J. Stabilization of constraints and integrals of motion in dynamical systems. *Comput Methods Appl Mech Eng*, 1972, 1: 1–16

## Appendix A

According to (23), the matrix  $\mathbf{A} = [\mathbf{A}_1, \mathbf{A}_2] \in \mathbb{R}^{11 \times 6}$  is defined as

$$\mathbf{A}_1 = \begin{bmatrix} \mathbf{J}_1^T \begin{bmatrix} c_1 \\ -s_1 \end{bmatrix} & \mathbf{0}_{4 \times 1} & -\frac{\partial}{\partial q_1} \varphi_{r_1} & \mathbf{0}_{4 \times 1} \\ \mathbf{0}_{4 \times 1} & \mathbf{J}_2^T \begin{bmatrix} -c_2 \\ s_2 \end{bmatrix} & \mathbf{0}_{4 \times 1} & -\frac{\partial}{\partial q_2} \varphi_{r_2} \\ -c_1 & c_2 & -J_{x_1} & -J_{x_2} \\ s_1 & -s_2 & -J_{y_1} & -J_{y_2} \\ 0 & 0 & R & -R \end{bmatrix}, \quad \mathbf{A}_2 = \begin{bmatrix} \bar{a}_1 \begin{bmatrix} s_1 \\ c_1 \end{bmatrix} & \mathbf{0}_{4 \times 1} & \frac{\beta_\theta}{D_L} \mathbf{J}_1^T \begin{bmatrix} y_1 - y_2 \\ x_2 - x_1 \end{bmatrix} \\ \bar{a}_2 \begin{bmatrix} s_2 \\ c_2 \end{bmatrix} & \mathbf{0}_{4 \times 1} & -\frac{\beta_\theta}{D_L} \mathbf{J}_2^T \begin{bmatrix} y_1 - y_2 \\ x_2 - x_1 \end{bmatrix} \\ J_{x_1} + J_{x_2} & 0 & 0 \\ J_{y_1} + J_{y_2} & 0 & 0 \\ 0 & -\frac{1}{2} R f_d D_{12} & 0 \end{bmatrix}$$

for  $\bar{a}_i = r_i D_i^{-1} \mathbf{J}_i^T$ ,  $J_{x_1} = \frac{\partial}{\partial \mathbf{x}} \varphi_{r_1}$ ,  $J_{y_1} = \frac{\partial}{\partial \mathbf{y}} \varphi_{r_1}$ ,  $J_{x_2} = \frac{\partial}{\partial \mathbf{x}} \varphi_{r_2}$ ,  $J_{y_2} = \frac{\partial}{\partial \mathbf{y}} \varphi_{r_2}$ .